

# Crystallinity estimation of thin silicon-on-insulator layers by means of diffractometry using a highly parallel X-ray microbeam

Shingo Takeda,<sup>a\*</sup> Kazushi Yokoyama,<sup>b</sup> Yoshiyuki Tsusaka,<sup>c</sup> Yasushi Kagoshima,<sup>c</sup> Junji Matsui<sup>c</sup> and Atsushi Ogura<sup>d</sup>

<sup>a</sup>Japan Synchrotron Radiation Research Institute, 1-1-1 Kouto, Sayo, Hyogo 679-5198, Japan,

<sup>b</sup>Hyogo Prefectural Center for Advanced Science and Technology, 3-1-1 Kouto, Kamigori, Ako, Hyogo 678-1205, Japan, <sup>c</sup>Graduate School of Material Science, University of Hyogo, 3-2-1 Kouto, Kamigori, Ako, Hyogo 678-1297, Japan, and <sup>d</sup>School of Science and Technology, Meiji University, 1-1-1 Higashisanda, Tama, Kawasaki, Kanagawa 214-8571, Japan. E-mail: stakeda@spring8.or.jp

An X-ray microbeam with a small angular divergence and a narrow energy bandwidth has been produced at BL24XU at SPring-8. The beam size was measured to be 3.1  $\mu\text{m}$  and 1.6  $\mu\text{m}$  in the horizontal and vertical directions, respectively, and the horizontal angular divergence was 4.0 arcsec. Using this microbeam the crystallinity estimation of thin layers on silicon-on-insulator (SOI) wafers is demonstrated. In reciprocal-space maps the lattice tilt variations were 80 arcsec and more than 220 arcsec in the SOI layers on bonded and SIMOX wafers, respectively. In equi-tilt maps, the typical equi-tilt areas of the SOI layers were 7  $\mu\text{m}$  and 4  $\mu\text{m}$  in size on the bonded and SIMOX wafers, respectively.

© 2006 International Union of Crystallography  
 Printed in Great Britain – all rights reserved

**Keywords:** silicon-on-insulator; thin layer; X-ray diffractometry; high-resolution diffraction; X-ray microbeam.

## 1. Introduction

Silicon-on-insulator (SOI) has been proposed as one of the advanced Si materials for metal-oxide semiconductor devices. The SOI layer is separated from the substrate by an oxidized layer. This structure can realise low-power and high-speed integrated circuits, such as complementary metal-oxide semiconductor (CMOS) devices. At present there are two typical technologies that form SOI layers, *i.e.* the bonded process and the process of separation by implanted oxygen (SIMOX) (Lasky, 1986; Izumi *et al.*, 1978). In both cases local strain and/or defects in the SOI layers may reduce the device performance or decrease its life span. Therefore, characterization of the crystalline quality of the top SOI layers is of great importance.

An X-ray microbeam is a powerful tool for measuring local strain concentration or uneven strain distribution, which may give rise to poor crystallinity in semiconducting materials. X-ray diffraction for local strain measurements using microbeams has already been reported, *e.g.* with the microbeams being produced by glass capillary (Rindby, 1986; Yamamoto, 1996), zone plate and waveguide (Cai *et al.*, 1999; Di Fonzo *et al.*, 2000). However, the microbeams produced by these methods have a low sensitivity for detecting minute strain in Si crystals. This is caused by the large angular

divergence of the microbeam compared with the intrinsic angular divergence of X-ray diffraction from a Si perfect crystal.

An optical system for producing an X-ray microbeam with both high angular and high spatial resolutions has been previously constructed using successive asymmetric Bragg reflections in both horizontal and vertical directions of incoming synchrotron X-rays (Tsusaka *et al.*, 2000). This microbeam achieved a size of 7.6  $\mu\text{m}$  (horizontal)  $\times$  5.7  $\mu\text{m}$  (vertical) and an angular divergence of less than 2 arcsec. However, the beam intensity of about  $10^5$  photons  $\text{s}^{-1}$  was insufficient to estimate the crystallinity of those thin layers. Here we describe a newly developed optical system able to provide high-flux photons, and estimation results for thin SOI layers using this system.

## 2. X-ray microbeam system

In order to measure the strain in a very local area in the SOI layers an X-ray microbeam with a small angular divergence and a narrow energy bandwidth has been fabricated. The optical system is schematically shown in Fig. 1. Synchrotron radiation was selected as the X-ray source and the X-ray energy was tuned to 15 keV using a monochromator. A four-quadrant slit positioned 66 m away from an undulator source

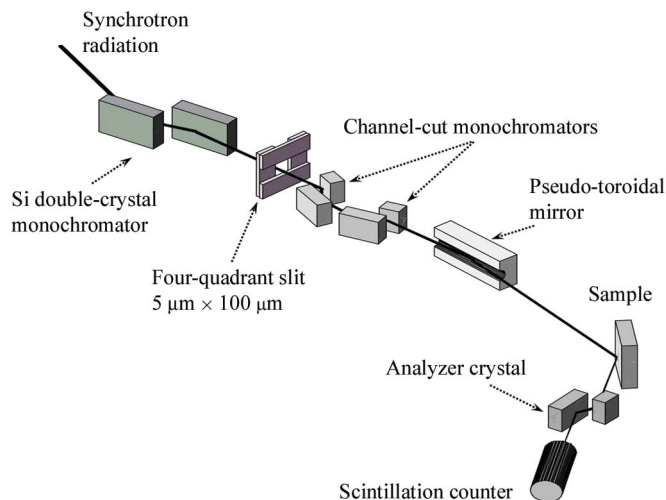


**Figure 1**  
Optical system of the parallel X-ray microbeam.

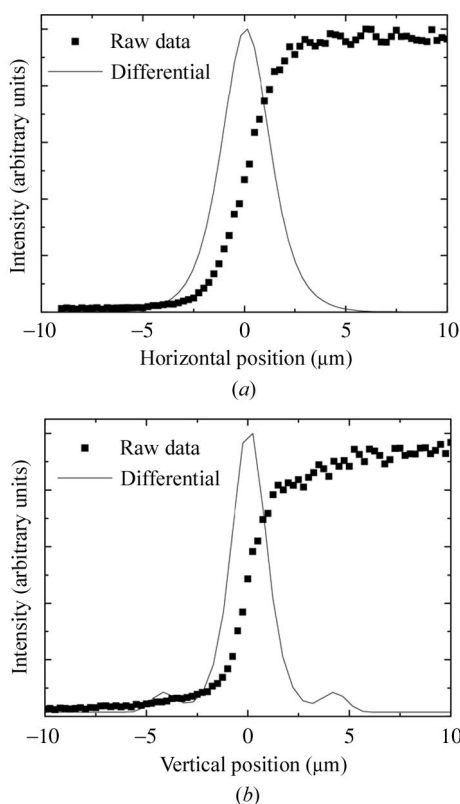


**Figure 2**  
Results of the beam size measurements. (a) Horizontal direction; (b) vertical direction. The dotted and solid lines represent the raw data and its differential, respectively.

was set to 5  $\mu\text{m}$  and 100  $\mu\text{m}$  in the horizontal and vertical directions, respectively. Four 333 reflections by two (111)-oriented channel-cut Si crystals with a (+, -, -, +) arrangement limited the energy spread to  $\Delta E/E \simeq 1 \times 10^{-5}$ . A rhodium-coated pseudo-toroidal mirror, which was configured by bending a cylindrical mirror, focuses X-rays onto the sample. The mirror has a concave curvature of about 8 mm. The mirror bending mechanism results in a concave curvature of about 450 m in the horizontal direction. The grazing angle

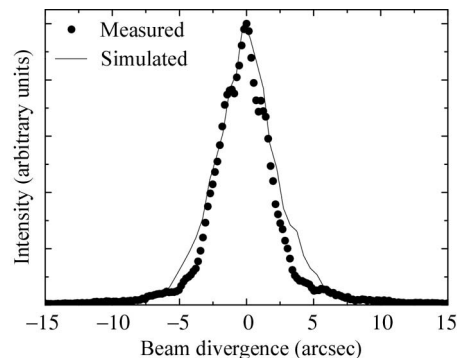


**Figure 3**  
Result of the rocking-curve measurements. The dotted and solid lines represent the measured data and ray-tracing calculations, respectively.

was 0.24° and the focal length was  $\sim 1$  m. The X-ray-illuminated area on the pseudo-toroidal mirror was restricted to  $\sim 1000 \mu\text{m} \times 100 \mu\text{m}$  by the four-quadrant slit. In this small area the figure difference between the pseudo-toroidal mirror and a paraboloid mirror was negligibly small. Because of the small illuminated area, the focused X-ray beam had a small angular divergence in the horizontal direction, sufficient to detect minute strains even in almost perfect crystals.

The focused X-ray beam using this optical system was simulated by the ray-tracing method. This resulted in simulated beam sizes at the sample position being estimated as 1.7  $\mu\text{m}$  and 0.5  $\mu\text{m}$  in the horizontal and vertical directions, respectively. The simulated beam has an angular divergence of 4.0 arcsec in the horizontal direction, which corresponds to a strain sensitivity of  $\Delta d/d_{004} \simeq 4.0 \times 10^{-5}$  for Si crystals. The vertical angular divergence was 21.5 arcsec, which was about ten times larger than that of the optical system using successive asymmetric Bragg reflections.

The X-ray microbeam has been produced at BL24XU at SPring-8. The horizontal and vertical beam sizes at the sample position were measured to be 3.1  $\mu\text{m}$  and 1.6  $\mu\text{m}$ , respectively, by the knife-edge scan method (Fig. 2). The demagnifications of the mirror were 0.6 $\times$  (horizontal) and 0.02 $\times$  (vertical). The measured horizontal and vertical beam sizes are about two and three times larger, respectively, than those obtained by the ray-tracing simulation, considered to be because of the roughness of the mirror surface. In order to estimate the horizontal beam divergence, we measured a rocking curve of the 115 asymmetric reflection of a silicon (001) crystal with a high incidence beam angle. Fig. 3 shows the resulting rocking-curve measurement. The angular divergence of the microbeam was estimated to be 4.0 arcsec, which is the same as the simulated value. The intensity was estimated to be  $\sim 5 \times 10^6$  photons  $\text{s}^{-1}$ .

### 3. Application to SOI characterization

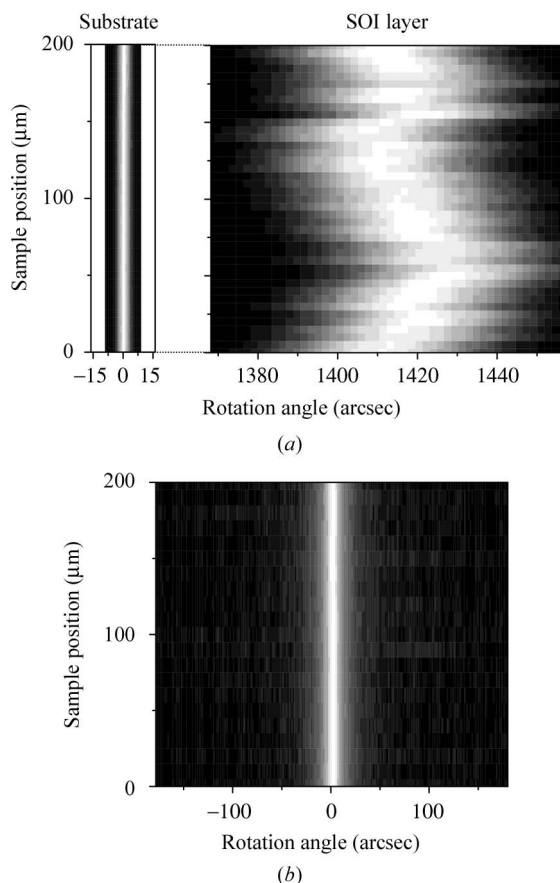
We then investigated the crystallinity of thin layers in the SOI wafers, using this microbeam. The SOI wafers used in the present measurement are listed in Table 1. Samples A and B are bonded SOI wafers having a 200 nm-thick and a 50 nm-thick SOI layer, respectively. Samples C and D are SIMOX

**Table 1**

List of estimated SOI wafers used in the experiment.

 $t_{\text{SOI}}$  and  $t_{\text{BOX}}$  indicate the thicknesses of the SOI and the BOX layers, respectively.

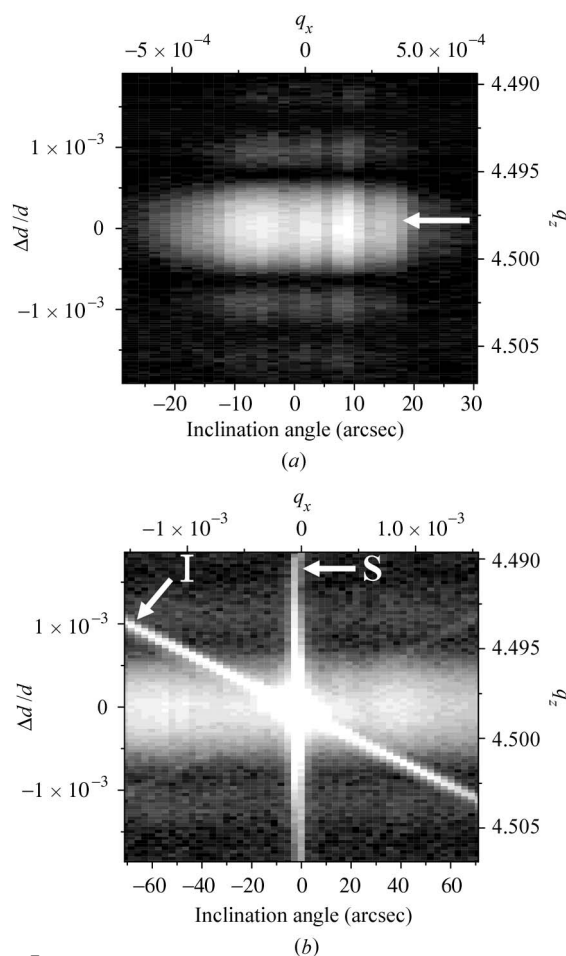
Layer	Process	$t_{\text{SOI}}$	$t_{\text{BOX}}$
A	Bonded	200 nm	400 nm
B	Bonded	50 nm	100 nm
C	SIMOX	170 nm	104 nm
D	SIMOX	52 nm	106 nm


**Figure 4**

Contour maps of the 004 diffraction intensity. The vertical axes gives the position of the silicon wafer. (a) Rocking curves for a 200 nm-thick bonded layer. (b) Rocking curves for a 200 nm-thick SIMOX layer.

wafers having thicknesses of 170 nm and 52 nm, respectively. These samples have a buried oxide (BOX) layer of about 100 nm thickness, except for sample A (400 nm-thick).

Rocking curves for these samples were obtained in a similar way to that reported previously (Tsusaka *et al.*, 2003). Fig. 4 shows a contour map of a set of 004 rocking curves obtained by scanning the sample in the vertical direction with 5 mm step widths. The illuminated area on the sample surface was 9.9  $\mu\text{m}$  (horizontal)  $\times$  1.6  $\mu\text{m}$  (vertical) at an incidence Bragg angle of 17.7°. The extinction distance was calculated to be 1.7  $\mu\text{m}$ . The vertical and horizontal axes in Fig. 4 represent the position ( $z$ ) and rotating angle ( $\omega$ ) of the SOI wafer, respectively. The left-hand and right-hand diffraction peaks in Fig. 4(a) are from the substrate and the SOI layer, respectively. The angular


**Figure 5**

Reciprocal-space maps for (a) a 200 nm-thick bonded layer and (b) a 200 nm-thick SIMOX layer.

separation between the two diffraction peaks resulted from unintentional tilt of the 001 lattice plane of the SOI layer from that of the Si substrate. This is very usual for bonded SOI wafers. In the case of sample C, as seen in Fig. 4(b), only one peak appears, indicating that the lattice plane of the SIMOX SOI layer is parallel to that of the substrate (Shimura *et al.*, 2000).

By adding an analyzer crystal placed behind the sample into the X-ray path, two-dimensional  $\omega$ - $2\theta$  maps (*i.e.* reciprocal-space maps) were drawn in triple-axis mode (Fewster, 1993). The 333 reflections of a (111)-oriented channel-cut Si crystal were selected for the analyser of that system. Fig. 5(a) shows a reciprocal-space map near the 004 lattice point for sample A. The reflection intensity of the main peak in Fig. 5(a) (as indicated by the arrow) spreads out in the horizontal direction. On both sides of the main peak one can see more than two satellite peaks (so-called ‘thickness fringes’) (Shimura *et al.*, 2000). Since these peaks are usually observed in thin crystals, the intensity distribution can be safely said to have originated from the SOI layer.

Fig. 5(b) shows a reciprocal-space map for C. In addition to the main peak and the thickness fringes, the intensity distribution in the  $q_x$  direction is more widely spread than that for sample A (Fig. 5a). A vertically spread intensity distribution

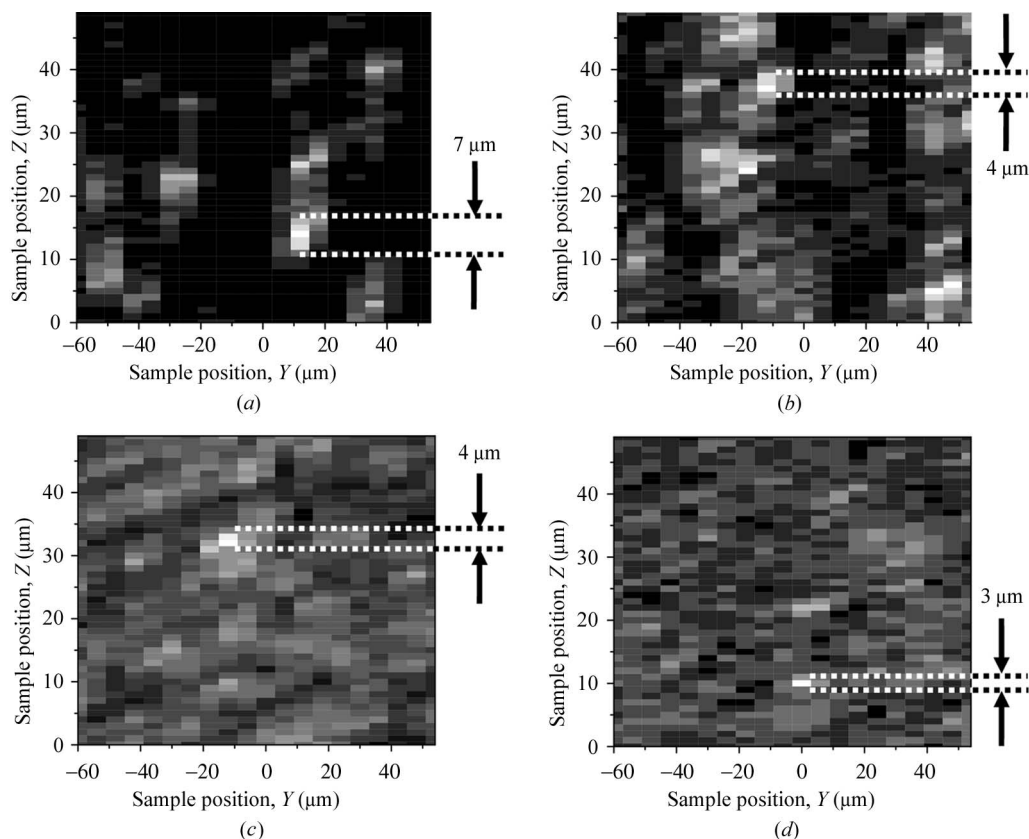


**Figure 6** Equi-tilt maps for (a) a 50 nm-thick bonded layer, (b) a 200 nm-thick bonded layer, (c) a 50 nm-thick SIMOX layer, and (d) a 200 nm-thick SIMOX layer.

(indicated by arrow S) and obliquely elongated intensity distribution (indicated by arrow I) are clearly seen. The former intensity distribution (S) is derived from the substrate and the latter (I) is due to the angular divergence of the incident X-ray beam. This situation holds true only for the case where the substrate quality is very high. Intensity distributions in the  $q_x$  direction for both the main peak and the satellite peaks in Figs. 5(a) and 5(b) show the existence of a lattice tilt variation.

Here we define the crystal region as having the same lattice plane tilt and the same lattice spacing as an ‘equi-tilt area’. The sizes of the equi-tilt areas in the SOI layer were measured using the following method. First, the sample and the analyser crystal were set at fixed  $\omega$  and  $2\theta$  angles, respectively, *i.e.* the X-ray reflection intensity was measured at a fixed point in the reciprocal space. Then the sample was scanned parallel to the sample surface giving an equi-tilt area map, from which one can determine the two-dimensional distribution of the crystal regions of the same lattice tilt and of the same lattice spacing. Fig. 6 shows equi-tilt area maps of the SOI layer in a  $100\ \mu\text{m} \times 50\ \mu\text{m}$  area with scanning steps of  $6\ \mu\text{m}$  (horizontal) and  $1\ \mu\text{m}$  (vertical). The largest equi-tilt area sizes were found to be  $7\ \mu\text{m}$  and  $4\ \mu\text{m}$  for 200 nm-thick and 50 nm-thick bonded SOI layers, respectively, and  $4\ \mu\text{m}$  and  $3\ \mu\text{m}$  for 170 nm-thick and 52 nm-thick SIMOX SOI layers, respectively.

In this experiment the crystallinity of the SOI layers in both SOI wafers was found to be inferior to that of the Si substrate.

This situation might be caused by some stresses being exerted unintentionally during the wafer fabrication processes, such as surface polishing and uneven temperature distribution in a single wafer, in addition to the difference in thermal expansion coefficients.

#### 4. Summary

An X-ray microbeam with small angular divergence and narrow energy bandwidth has been obtained using a pseudotoroidal mirror and Si channel-cut crystals. The size of the microbeam was  $3.1\ \mu\text{m}$  in the horizontal and  $1.6\ \mu\text{m}$  in the vertical direction, and the angular divergence was 4.0 arcsec. Using the microbeam the crystallinity of the thin bonded and SIMOX layers of the SOI wafers was evaluated in terms of the lattice tilt variation and the lattice spacing variation.

This work was performed at SPring-8 with the approval of the Japan Synchrotron Radiation Research Institute (JASRI) (proposal No. C03B24XU-5043N).

#### References

- Cai, Z. *et al.* (1999). *Appl. Phys. Lett.* **75**, 100–102.
- Di Fonzo, S., Jark, W., Lagomarsino, S., Giannini, C., De Caro, L., Cedola, A. & Muller, M. (2000). *Nature (London)*, **403**, 638–640.

- Fewster, P. F. (1993). *Semicond. Sci. Technol.* **8**, 1915–1934.
- Izumi, K., Doken, M. & Ariyoshi, H. (1978). *Electron. Lett.* **14**, 593–594.
- Lasky, B. (1986). *Appl. Phys. Lett.* **48**, 78–80.
- Rindby, A. (1986). *Nucl. Instrum. Methods*, **A249**, 536–540.
- Shimura, T., Hosoi, T. & Umeno, M. (2000) *J. Cryst. Growth*, **210**, 98–101.
- Tsusaka, Y., Urakawa, M., Yokoyama, K., Takeda, S., Katou, M., Kurihara, H., Yoshida, F., Watanabe, K., Kagoshima, Y. & Matsui, J. (2003). *Nucl. Instrum. Methods*, **B199**, 19–22.
- Tsusaka, Y., Yokoyama, K., Takeda, S., Urakawa, M., Kagoshima, Y., Matsui, J., Kimura, S., Kimura, H., Kobayashi, K. & Izumi, K. (2000). *Jpn. J. Appl. Phys.* **39**, 635–637.
- Yamamoto, N. (1996). *Rev. Sci. Instrum.* **67**, 3051–3064.